Heliyon 9 (2023) e21695

Contents lists available at ScienceDirect

Heliyon

journal homepage: www.cell.com/heliyon

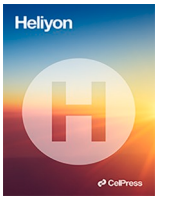

SIRT1-dependent mitochondrial biogenesis supports therapeutic effects of vidarabine against rotenone-induced neural cell injury

Lanxin Li [a,1], Yang Zhang [b,1], Zhengqian Chen [a,c], Ruyong Yao [a], Zhongqiu Xu [a,b], Can Xu [a,b], Fujie He [b], Haitao Pei [d,**], Cui Hao [a,*]

[a] Medical Research Center, the Affiliated Hospital of Qingdao University, Qingdao, 266003, China
[b] Key Laboratory of Marine Drugs, Ministry of Education, Ocean University of China, Qingdao 266003, China
[c] Department of Orthopedics, Qingdao Chengyang Guzhen Orthopaedic Hospital, Qingdao, 266107, China
[d] Department of Neurology, the Affiliated Hospital of Qingdao University, Qingdao, 266003, China

ARTICLE INFO

Keywords:
Parkinson's disease
SH-SY5Y cells
mitochondrial biogenesis
oxidative stress
SIRT1

ABSTRACT

Parkinson's disease (PD) is the second most common neurodegenerative disease in the world, which is distinguished by the loss of dopaminergic (DA) neurons in the substantia nigra and the formation of intraneuronal. Numerous studies showed that the damage and dysfunction of mitochondria may play key roles in DA neuronal loss. Thus, it is necessary to seek therapeutic measures for PD targeting mitochondrial function and biogenesis. In this study, through screening the purchased compound library, we found that marine derived vidarabine had significant neuroprotective effects against rotenone (ROT) induced SH-SY5Y cell injury. Further studies indicated that vidarabine pretreatment significantly protected ROT-treated SH-SY5Y cells from toxicity by preserving mitochondrial morphology, improving mitochondrial function, and reducing cell apoptosis. Vidarabine also reduced the oxidative stress and increased the expression levels of PGC-1α, NRF1, and TFAM proteins, which was accompanied by the increased mitochondrial biogenesis. However, the neuroprotective effects of vidarabine were counteracted in the presence of SIRT1-specific inhibitor Ex-527. Besides, vidarabine treatment attenuated the weight loss, alleviated the motor deficits and inhibited the neuronal injury in the MPTP induced mouse model. Thus, vidarabine may exert neuroprotective effects via a mechanism involving specific connections between the SIRT1-dependent mitochondrial biogenesis and its antioxidant capacity, suggesting that vidarabine has potential to be developed into a novel therapeutic agent for PD.

1. Introduction

Parkinson's disease (PD) is the most common age-related motoric neurodegenerative disease caused by the selective loss of dopaminergic (DA) neurons in the substantia nigra of the brain, characterized by nigrostriatal degeneration and the spreading of aggregated forms of the presynaptic protein α-synuclein (α-syn) [1]. Although the causative mechanisms of PD pathogenesis are still

* Corresponding author
** Corresponding author
E-mail addresses: peihtao@163.com (H. Pei), haocui@qduhospital.cn (C. Hao).
[1] These authors contributed equally to this work.

https://doi.org/10.1016/j.heliyon.2023.e21695
Received 25 July 2023; Received in revised form 8 September 2023; Accepted 25 October 2023
Available online 26 October 2023

unclear, numerous studies have shown that the neuroinflammation and dysfunction of mitochondria may play key roles in DA neuronal loss. However, until now there is still a lack of viable medications that can block or postpone PD neurodegeneration. Thus, it is urgent to develop novel therapeutic measures for the prevention and therapy of PD.

Mitochondria is the main source of energy and endogenous ROS in the body, and plays a key role in the function and survival of neurons in the brain [2]. Mitochondrial dysfunction has long been recognized as a key pathogenic hallmark and the primary etiology of PD [3,4]. Maintaining a healthy mitochondrial pool in cells, particularly neurons, is crucial for the normal function of the nervous system [3]. Mitochondrial biogenesis, a process that new mitochondria are formed by the growth and division of pre-existing mitochondria, can increase the mitochondrial mass and maintain the morphology of mitochondria. The major regulator of mitochondrial biogenesis is peroxisome-proliferator-activated γ co-activator-1α (PGC-1α), which can stimulate the nuclear respiratory factors 1 and 2 (NRF-1 and NRF-2) so as to activate various mitochondrial genes such as mitochondrial transcription factor A (TFAM) that is necessary for mitochondrial DNA (mtDNA) transcription and replication [5–7]. Accordingly, enhancing the mitochondrial biogenesis offers a promising therapeutic target in neurodegenerative disease.

Vidarabine (9-β-D-arabinofuranosyladenine), a adenosine analogue, is initially isolated from Caribbean sponge in the 1960s and later isolated by Parke, Davis and Company (British Patent No. 1,159, 290) as a marine derived medicine [8,9]. Initially developed as an antineoplastic drug, and it was later known for its superior activity against the herpes virus and was the first marine antiviral nucleoside analog [8,9]. Recent studies have demonstrated that vidarabine has specific adenylyl cyclase 5 (AC5) inhibitory effects, which not only slow the development of heart failure (HF) but also cause less cardiac depression in mice [10]. Vidarabine can also mimic the salutary effects of AC5 disruption on cancer prevention and protects against tumor growth in syngeneic mouse models [11]. Notably, a series of studies demonstrated that vidarabine's anti-oxidant impact on cardiomyocytes, lending credence to the idea that vidarabine may be effective in the treatment of many disorders induced by oxidative stress and mitochondrial dysfunction [10–12]. However, until now, there has been minimal research on vidarabine in the neurological field. In this study, we established the ROT-induced PD cell model to screen the purchased compound library, and discovered that vidarabine possessed significant neuroprotective effects against rotenone (ROT) induced SH-SY5Y cell injury. Then the protective effect and molecular mechanism of vidarabine against neural cell damage were further investigated. The results indicated that vidarabine may attenuate the ROT-induced SH-SY5Y cell damage via utilizing SIRT1-dependent mitochondrial biogenesis and lowering the oxidative stress.

2. Materials and methods

2.1. Chemicals

Vidarabine (purity 99 %, CAS: 5536-17-4) was purchased from Targetmol USA (Shanghai, China). Dimethyl sulfoxide was obtained from Sigma (St. Louis, Missouri, USA). Rotenone (ROT, 95 % purity, CAS: 83-79-4) was bought from BD Biosciences (Shanghai, China). Methyl viologen dichloride was purchased from Aladdin (Shanghai, China). Dulbecco's modified Eagle medium (DMEM) was from Procell (Wuhan, China). Fetal bovine serum was from ExCell Bio (Shanghai, China). Resazurin (CAS: 62758-13-8) was from Solarbio (Beijing, China). The NAD^+/NADH assay kit with WST-8, lipid peroxidation malondialdehyde (MDA) assay kit、total antioxidant capacity assay kit, total superoxide dismutase assay kit with NBT, GSH and GSSG assay kit, the apoptosis and necrosis detection kit with YO-PRO-1 and PI, Mito-Tracker Red CMXRos probe, Mito-Tracker Green probe, YO-PRO-1/PI apoptosis detection kit and Hoechst 33342 staining solution were obtained from Beyotime Biotechnology (Shanghai, China). Seahorse XF Cell Mito Stress Test (103015–100) was from Agilent Technologies (Santa Clara, CA, USA). PGC-1α (1:5000, Cat No. 66369-1-Ig), SIRT1 (1:1000, Cat No. 13161-1-AP) were bought from Proteintech Group (Wuhan, China). NRF1 (1:1000, Cat No. E-AB-16661), and TFAM (1:1000, Cat No. 22586-1-AP) were purchased from Elabscience (Wuhan, China).

2.2. Cell culture and drug treatment

The human neuroblastoma (SH-SY5Y) cells were obtained as a gift from Prof. Xiangping Liu of the Affiliated Hospital of Qingdao University, and cultured in DMEM supplemented with 10 % fetal bovine serum (FBS, Gibco), 100 U/mL penicillin, and 100 μg/mL streptomycin. SH-SY5Y cells were subcultured or seeded onto plates until about 90 % confluence using the trypsin EDTA (Gibco) method. Cells in the control group were incubated with normal growth conditions. Cells in the ROT group were incubated for 24 h in media containing 20 μM ROT. The cells in the vidarabine pretreatment groups were cultivated in media containing varying doses of vidarabine (7.5, 15, and 30 μM) for 2 h before being incubated with a medium containing 20 μM ROT for 24 h. Thirty minutes before ROT and vidarabine treatment, the SIRT1 inhibitor EX-527 (10 μM) was added to the cells in the Ex-527 group.

2.3. Detection of cell viability

The cell viability of SH-SY5Y cells was determined using the resazurin assay [13]. Briefly, after 24 h of drug treatment, 20 μL of resazurin at a final concentration of 0.2 mg/mL was added to each well and incubated for 6.5 h at 37 °C. The fluorescence was then measured with a TECAN Infinite® 200 PRO plate reader (TECAN, Switzerland) at 544 and 595 nm for excitation and emission, respectively. Cell viability was calculated as a percentage of the non-treated control group. In addition, the cell morphology was observed after 24 h of incubation by using the inverted microscope fitted with a Revolve microscope (RVL-100-G, Echo Laboratories, San Diego, US).

2.4. Cell apoptosis and necrosis assay

Propidium Iodide (PI) can only stain the necrotic cells with lost membrane integrity, while YO-PRO-1 (YP1) can detect both the apoptotic and necrotic cells [14]. Briefly, SH-SY5Y cells were seeded at a density of 5×10^3 cells/well in a 96-well plate. After drug treatment for 24 h, the culture medium was aspirated, and the cells were washed once with PBS before being incubated with 100 μL of assay working solution containing 0.1 μL of YP1 and 0.1 μL of PI for 10 min at 37 °C. After incubation, the stained cells were observed under the fluorescence microscopy (RVL-100-G, Echo Laboratories, San Diego, US) (YP1, Ex/Em = 491/509 nm; PI, Ex/Em = 535/617 nm).

2.5. Determination of MDA, SOD, GSH, and total antioxidant activity in SH-SY5Y cells

SH-SY5Y cells were seeded at a density of 2×10^5 cells per well in 6-well plates. The medium was emptied and washed with 1 x PBS after 24 h of continuous culture. The cells were collected and the protein content of the sample was measured using the BCA kit. After that, the MDA (malondialdehyde peroxide) test kit, total antioxidant capacity assay kit, total superoxide dismutase (SOD) assay kit, and GSH assay kit were used to determine the MDA content, the total antioxidant capacity, the SOD content, and the GSH content, respectively, according to the manufacturer's protocols (Beyotime, Shanghai, China).

2.6. Determination of NAD^+/NADH ratio

The NAD^+/NADH Assay Kit with WST-8 was used to determine the NAD^+ and NADH content, according to the manufacturer's protocols (Beyotime, Shanghai, China). SH-SY5Y cells were seeded at a density of 2×10^5 cells/well in 6-well plates. The culture media was withdrawn after 24 h of treatment per group before being washed with PBS once, and then the cells were lysed according to the instructions, and the supernatant was collected. The samples to be analyzed were placed in 96-well plates and incubated for 10 min at 37 °C before adding 10 μL of a chromogenic solution to each well. Following a 30-min incubation at 37 °C, the absorbance at 450 nm was measured with a TECAN Safire multipurpose microplate meter to determine the total quantity of NAD^+ and NADH in the sample.

2.7. Determination of the mass and activity of mitochondrial

Mito-Tracker Green is largely insensitive to MMP and oxidative stress [15], whereas Mito-Tracker Red CMXRos can precisely mark active mitochondria [16]. Mitochondrial activity and quality were assessed by utilizing these two probes at the same time. Briefly, the SH-SY5Y cells were incubated, seeded, and grouped as described above, then washed with PBS and stained with 100 nM Mito-Tracker Red CMXRos, 200 nM Mito-Tracker Green, and Hoechst 33342 according to the manufacturer's protocols (Beyotime, Shanghai, China). Then the cells were incubated for 30 min at room temperature (20–25 °C) without light before placing them in an ice bath. After that, the cells were then examined using fluorescence microscopy (RVL-100-G, Echo Laboratories, San Diego, US). The images were taken to estimate the average fluorescence intensity in the cells, which was then used to calculate the activity and mass of mitochondria.

2.8. Measurement of mitochondrial membrane potential (MMP)

JC-1 is a popular fluorescent probe for measuring the mitochondrial membrane potential (MMP). In healthy cells with functioning mitochondria, the mitochondrial membrane potential is high, so the JC-1 aggregates display red fluorescence (Ex/Em = 585/590 nm). However, in MMP-depleted apoptotic cells, very tiny quantities of JC-1 can enter the mitochondria and show the green fluorescence of JC-1 monomers (Ex/Em = 515/529 nm). The MMP of cells in each treatment group was assessed by using the JC-1 MMP assay kit (Beyotime, Shanghai, China) according to the operating manual. In brief, the cells were washed with FBS once and then incubated with JC-1 (200 μM) for 20 min at 37 °C before rinsed with FBS to eliminate the excess JC-1. Finally, the confocal microscopy was used to obtain the fluorescence pictures of JC-1 in SH-SY5Y cells.

2.9. Measurement of mitochondrial function seahorse XFp extracellular flux analyzer

The function of mitochondria was evaluated by using the Seahorse XFp Extracellular Flux Analyzer to assess the oxygen consumption rate (OCR) (Seahorse Bioscience, MA, USA). In brief, the cells were grown in DMEM media at 37 °C in a 5 % CO_2 incubator for 24 h on XFp cell culture miniplates (Seahorse Bioscience, MA, USA) (2×10^4 cells/well). The media was then withdrawn, and the cells were washed twice with an XF assay medium (Seahorse Bioscience, MA, USA). Then the cells were cultured for 1 h in an XF assay medium at 37 °C without CO_2 to achieve temperature and pH balance. In the XF assay medium, mitochondrial complex inhibitors (oligomycin, FCCP, and antimycin A/rotenone) were newly produced. A seahorse cartridge with detection probes was employed (Seahorse Bioscience, MA, USA). To inject oligomycin (1.5 μM), carbonyl cyano-*p*-trifluoromethoxy-phenylhydrazone (FCCP, 2 μM), and antimycin A (0.5 μM) into injection ports A, B, and C, respectively, a seahorse cartridge with detection probes (Seahorse Bioscience, MA, USA) was employed. Then the cells and reagents were then loaded into the analyzer. After monitoring the basal respiration, oligomycin (1.5 μM), which inhibits ATP synthase, was administered first to evaluate ATP-linked respiration and proton leak. Following that, FCCP (2.0 μM), which uncouples mitochondria, was added to isolate mitochondria and obtain maximal respiration and spare respiratory capacity. Finally, to suppress the mitochondrial respiration, a combination of antimycin A (0.5 μM), an

electron transport blocker, and rotenone (0.5 μM), an inhibitor of mitochondrial complex I, was administered. Following that, the number of cells in each well was counted using the trypsin EDTA method. OCR was recorded as pmol/min, and the normalized unit in this study was 1×10^3 cells.

2.10. Confocal fluorescence microscopy for mitochondrial morphology

SH-SY5Y cells seeded on the 20 mm confocal culture dish were incubated with 100 nM Mito-Tracker Red CMXRos for 15 min at 37 °C in the dark before visualization. Then the fluorescence was detected (Ex/Em = 579/599 nm) using the Confocal Fluorescence Microscopy (Nikon A1/N-SIM, Japan). Acquired images were quantified by using the Image J software. The form factor is calculated as follows: form factor (FF, defined as $(P^2)/(4\pi A)$, where P is the length of mitochondrial outline and A is the area of mitochondrion, aspect ratio (AR, the ratio between the major and minor axis of the ellipse equivalent to the mitochondrion), as previously reported [17]. The high FF values indicate the long and highly branched mitochondrial segments, while the high AR values are assigned to long and elliptical segments.

2.11. Protein extraction

Cells were inoculated in 6-well plates, and after group processing, SH-SY5Y cells were collected and lysed in pre-chilled RIPA buffer mixed with 1 mM PMSF (Beyotime, Shanghai, China) and centrifuged at 14,000 g for 5 min at 4 °C. The supernatant was removed and the protein concentration was measured using the BCA Protein Assay Kit (Beyotime, Shanghai, China). Samples were collected for the next step of western blotting experiments.

2.12. Western blot assay

SH-SY5Y cells were collected and lysed in pre-chilled RIPA buffer mixed with 1 mM PMSF (Beyotime, Shanghai, China) and centrifuged at 14,000 g for 5 min at 4 °C. The equivalent amounts of proteins from each sample were separated with 8–12 % SDS-polyacrylamide gel electrophoresis and transferred to the NC membrane according to the manufacturer's instructions (Millipore, Bedford, MA, USA). After that, the membrane was blocked for 1 h at room temperature (RT) with 5 % non-fat milk in Tris-buffered saline (TBST) and incubated overnight at 4 °C with the specified primary antibodies. The membranes were then washed and incubated with AP-labeled secondary antibody (1:2000 dilutions) at RT for 2 h. The protein bands were then visualized by incubating with the developing solution (p-nitro blue tetrazolium chloride (NBT) and 5-bromo-4-chloro-3-indolyl phosphate toluidine (BCIP)) at RT for 30 min. The relative densities of proteins were all determined by using ImageJ (NIH) v.1.33u (USA).

2.13. Animal experiments

2.13.1. Animals and experimental design

Six-to-ten-week-old male C57BL/6 mice weighing 20–25 g each were obtained from Orient Bio (Jinan, China). Five mice were housed in one cage under specific pathogen-free conditions. All mice were bred and maintained under a 12 h light/dark cycle with unrestricted access to food and water at a controlled temperature (22 ± 2 °C) and humidity (55 ± 5 %). All experimental animal procedures were conducted according to the National Institutes of Health Guide for the Care and Use of Laboratory Animals and were approved by the Experimental Animal Ethics Committee of Qingdao University (AHQU-MAL20230711). The schematic representation of the experimental procedure was shown in Fig. 7A. After three days of acclimation, mice were randomly divided into four groups: the control group (n = 5), which was treated with 0.9 % sterile saline by intraperitoneal injection from day 0 to day 14; MPTP group (n = 5), which was treated with MPTP (25 mg/kg/day) by intraperitoneal injection from day 8 to day 14; Vidarabine group (n = 5), which was treated with vidarabine (60 mg/kg/day) from day 0 to day 14 and MPTP (25 mg/kg/day) from day 8 to day 14 by intraperitoneal injection; Vidarabine + Ex527 group (n = 5), which was pretreated with Ex527 (10 mg/kg/day) 2 h before treatment with vidarabine (60 mg/kg/day) and MPTP (25 mg/kg/day) by intraperitoneal injection. The body weights of six mice in each group were monitored daily for 14 days [18].

2.13.2. Behavioral assessment

From day 15 to day 16, behavioral tests, such as pole test, traction test, and open field test were performed to assess the motor impairment of MPTP-induced PD mouse model.

2.13.2.1. Pole test. The pole test was used to assess bradykinesia and physical coordination of the PD mouse [18,19]. The straight wooden rod has a height of 50 cm and a diameter of 3 cm, and is wrapped in non-adhesive gauze with a wooden ball (diameter 4 cm) on the top. The apparatus was vertically placed in a plastic cage covered with bedding on the bottom. The mouse was placed head up on the ball and recorded the return time from the beginning of the movement to the complete downward movement of the body. The total time from the start of the movement to the bottom was also recorded.

2.13.2.2. Traction test. The traction test was used to assess equilibrium and muscle strength of mice [19]. The front paws of mice were placed on a smooth steel wire with a height of 30 cm, a diameter of 1.5 mm, and a length of 30 cm. After confirming that the mouse

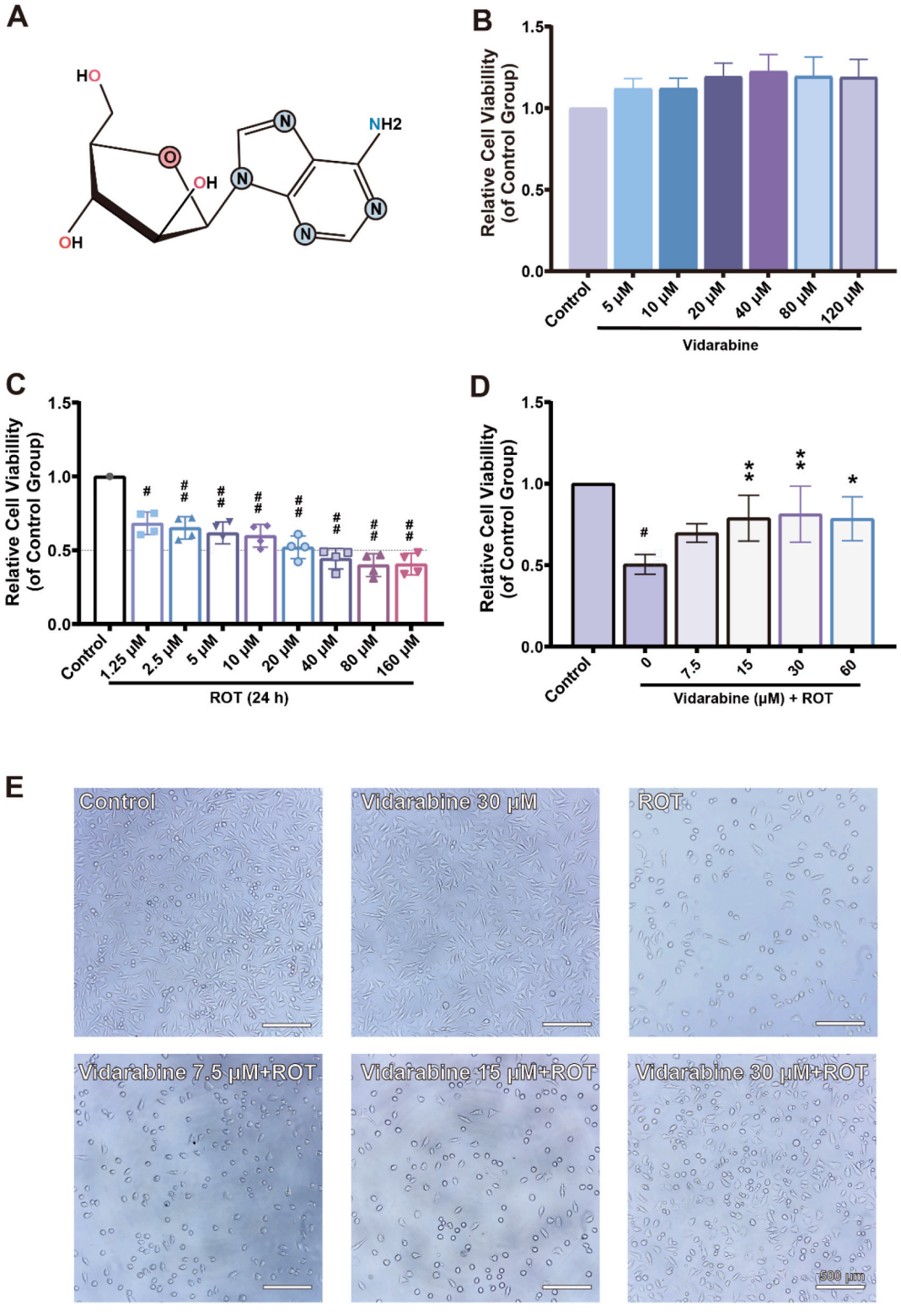

(caption on next page)

Fig. 1. Vidarabine protects SH-SY5Y cells against ROT-induced cell damage and morphological changes. (A) Chemical structure of Vidarabine. (B) Effect of Vidarabine on SH-SY5Y cell viability. Cell viability was assessed by the resazurin assay after 24 h of treatment with various concentrations of vidarabine. (C) Determination of the optimal concentration of the ROT effect. The cell viability was assessed by the resazurin assay after 24 h of treatment with various concentrations of ROT. (D) Protective effects of vidarabine against ROT-induced cell injury in SH-SY5Y cells. SH-SY5Y cells were pretreated with vidarabine for 2 h and then stimulated with 20 μM ROT for 24 h. Cell viability was measured using the resazurin assay. (E) Morphological alterations in SH-SY5Y cells. SH-SY5Y cells were treated for 24 h with vidarabine (7.5, 15, 30 μM) in the presence of 20 μM ROT. Scale bar = 500 μm. The data are represented as the mean ± SEM. $\#P < 0.05$, $\#\#P < 0.01$ compared with the control group; $*P < 0.005$, $**P < 0.01$ compared with the ROT group.

tightly grasps, record the time from release to mouse drop. Each mouse was tested three times with an interval of 1 h and then the mean value was calculated for subsequent analysis.

2.13.2.3. Open field test. The open field test was performed to evaluate spontaneous locomotor activity of the PD mouse [19,20]. Prior to the test, mice were transferred to the experimental room and adapted for at least 30 min. The square arena of the cubic box (45 × 45 × 45 cm) being divided into 16 equal rectangles by lines. The mouse was placed in the fixed position of the arena and allowed to move freely for 5 min and the Morris video analysis system (ZS Morris, Zhongshidichuang, Beijing, China) records the motion trajectory. A series of parameters, including tracks of movement patterns, total distance traveled and the number of crossing lines were analyzed by the Labmaze animal behavior analysis software (Zhongshidichuang, Beijing, China). To eliminate interference, the open field was cleaned with 75 % ethanol before and after each test.

2.13.3. Histopathological analysis

In order to analyze the histopathological changes, the mice were anesthetized with isoflurane gas, euthanized, and their brains were separated [21]. The brain tissues were fixed by immersion in 4 % (w/v) formaldehyde for 48 h at room temperature before embedded in paraffin and sectioned (4 mm). Then the paraffin sections were stained by hematoxylin & eosin (HE), and the brain histopathologic changes were examined by light microscopy.

2.14. Statistical analysis

All data are representative of at least three independent experiments. Data are presented as mean ± SEM, and the statistical analyses were performed by using the Prism 9.0 software. One-way ANOVA (analysis of variance) followed by Tukey's *post hoc* tests was performed to compare mean values of multiple groups. $P < 0.05$ was considered statistically significant.

3. Results

3.1. Vidarabine protects rotenone-induced SH-SY5Y cell's viability and ameliorates its morphology

Vidarabine, a marine derived medicine (Fig. 1A), was the first intravenous antiviral drug to be approved for widespread clinical use [22]. Rotenone can induce the neurodegeneration in SH-SY5Y cells and has been widely used to establish the *in vitro* model of PD. The cytotoxicity of vidarabine was first evaluated by resazurin assay and the results showed that vidarabine at the concentrations from 5 to 120 mM did not have any toxic effects on SH-SY5Y cells (Fig. 1B). In order to confirm an optimal damage concentration of ROT-induced *in vitro* PD model, various concentrations of rotenone (1.25–160 μM) were exposed to SH-SY5Y cells to determine the degree of cell damage by the resazurin assay. The results indicated that rotenone treatment can dose-dependently reduce the cell viabilities and rotenone treatment with the concentration of 20 μM resulted in about 50 % cell death (Fig. 1C). Thus, rotenone of 20 μM was selected for all the subsequent experiments.

The protective effects of vidarabine against neurologic damage stimulated by rotenone were then evaluated in SH-SY5Y cells by the resazurin assay. As shown in Fig. 1D, vidarabine (15–60 μM) treatment significantly protects SH-SY5Y cells from ROT-induced cell death and increased the cell viability as compared to the ROT-treated control group without vidarabine treatment. Moreover, the results of morphological observation showed that ROT treatment significantly reduced the number of surviving cells and increased the number of round cells with the reduction in protrusions (Fig. 1E). However, vidarabine treatment resulted in a significant reversal of these abnormal cellular morphological changes (Fig. 1E). Taken together, these results suggested that vidarabine has cytoprotective properties by restoring the viability of the cells and improving the morphology of the cells.

3.2. Vidarabine reduced oxidative stress and ameliorate ROT-induced apoptosis SH-SY5Y cells

Rotenone is reported to be able to induce apoptosis in SHSY5Y cells, which can lead to cell damage [23]. Thus, we next investigated the protective effect of vidarabine against rotenone-induced apoptosis and necrosis using YO-PRO-1 and PI dyes staining. As shown in Fig. 2A, after 24 h of incubation with ROT, SH-SY5Y cells displayed the increased apoptosis and necrosis, indicated by the bright green and red fluorescence. In contrast, pretreatment with various concentrations of vidarabine (7.5–30 μM) for 2 h dramatically reduced the proportion of apoptotic and necrotic cells, consistent to the previous results of the resazurin assay (Fig. 2A).

Oxidative stress is thought to be the common underlying mechanism leading to cellular dysfunction and death in both idiopathic

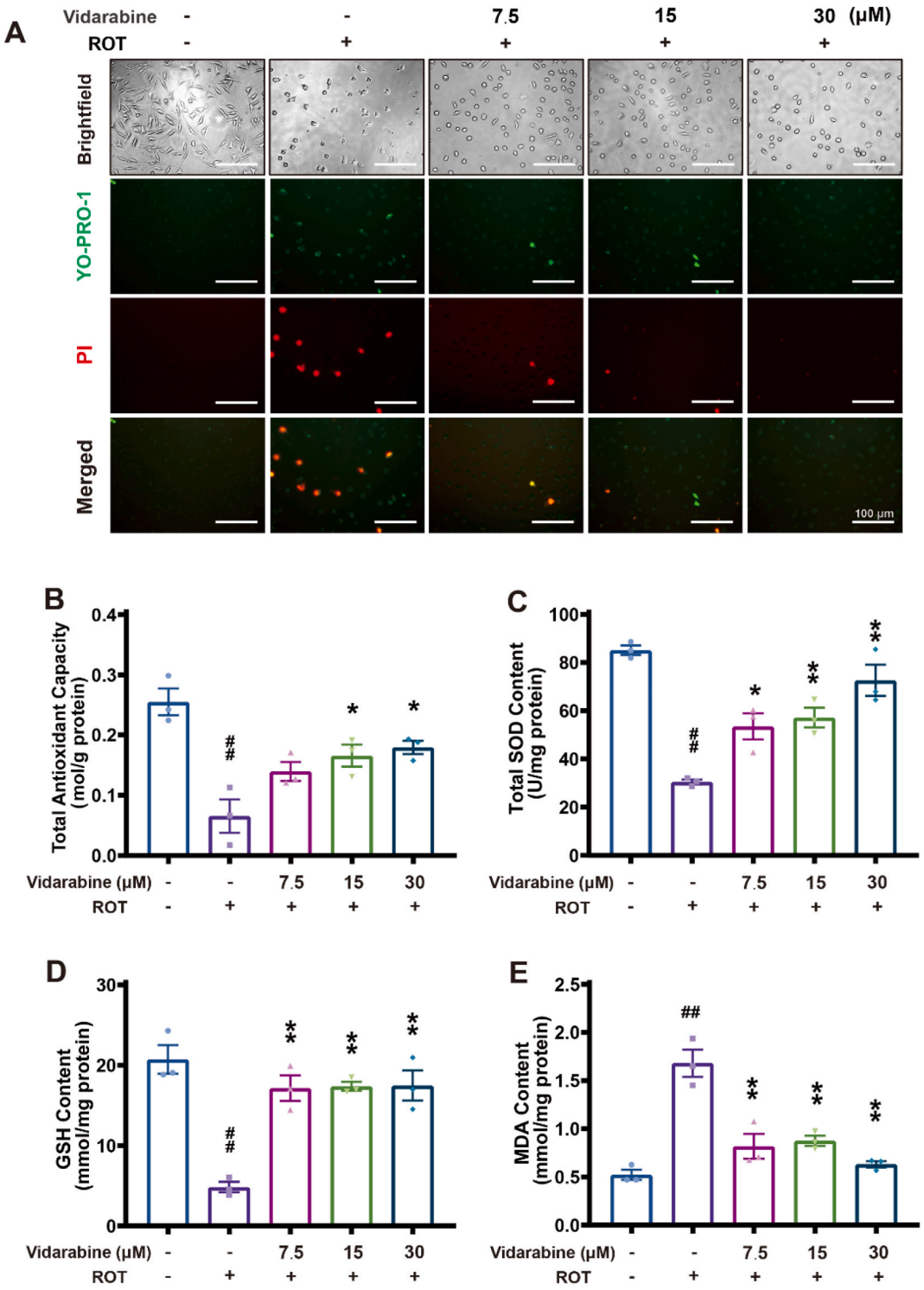

Fig. 2. Vidarabine reduced oxidative stress and ameliorated ROT-induced apoptosis in SH-SY5Y cells. (A) The necrosis or apoptosis of cells was detected by using YO-PRO-1 and PI staining. Scale bar = 100 μm. (B–E) The total antioxidant capacity (B), total SOD content (C), GSH content (D), and MDA levels (E) were evaluated by ELISA assay. The data are represented as the mean ± SEM (n = 3), $\#\#P < 0.01$ compared with the control group; $*P < 0.05$, $**P < 0.01$ compared with the ROT group.

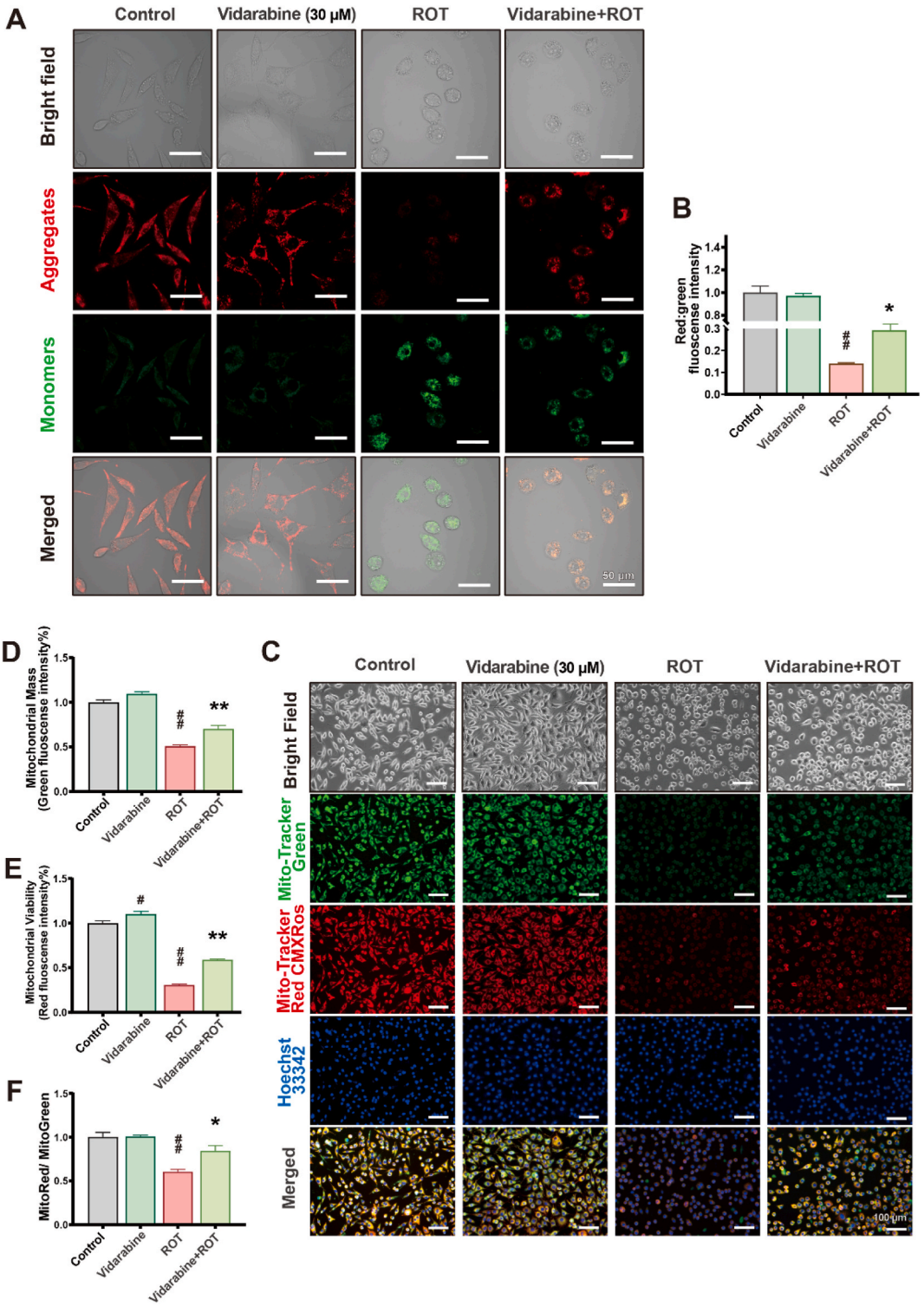

(caption on next page)

Fig. 3. Vidarabine alleviated the rotenone-induced mitochondrial damage. (A) SH-SY5Y cells were pretreated with or without vidarabine (30 μM) for 2 h and then stimulated with 20 μM ROT for 24 h. Then the changes in the mitochondrial membrane potential (MMP) were examined using the JC-1 staining. Scale bar = 50 μm. (B) Quantification analysis of JC-1 staining was performed to calculate the red/green fluorescence intensity ratio by Image J software. (C) Changes in the mitochondrial mass and viability were examined using the Mito-Tracker Green and Mito-Tracker Red CMXRos staining. Scale bar = 100 μm. (D–F) Quantitative analysis of mitochondrial mass (D), mitochondrial viability (E), and the ratio of MitoRed to MitoGreen fluorescence intensity (F) were performed by using Image J. Data are represented as the mean ± SEM, $\#P < 0.05$, $\#\#P < 0.01$ compared with the control group; $*P < 0.05$, $**P < 0.01$ compared with the ROT group. (For interpretation of the references to colour in this figure legend, the reader is referred to the Web version of this article.)

and genetic PD [24]. We then investigated the effects of vidarabine on rotenone-induced oxidative stress. The main biomarkers of oxidative stress including the Malondialdehyde (MDA), glutathione (GSH) content, total antioxidant capacity (T-AOC), and the superoxide dismutase (SOD) activities were evaluated by ELISA assay. As shown in Fig. 2B–E, ROT treatment of SH-SY5Y cells significantly increased the MDA content and reduced the total antioxidant capacity, GSH content, and total SOD content, verifying that rotenone treatment can truly induce the oxidative stress. However, after vidarabine treatment (7.5–30 μM), the MDA content significantly decreased while the cells' total antioxidant capacity, GSH content, and total SOD content significantly increased, as compared to the ROT-treated control group ($P < 0.05$) (Fig. 2B–E). Therefore, vidarabine can not only reduce the oxidative stress but also protect SH-SY5Y cells against ROT-induced cell apoptosis.

3.3. Vidarabine restored the ROT-induced mitochondrial membrane potential (MMP) depletion and improved the mitochondrial mass and viability

Mitochondria have been considered to play a key role in the apoptotic process [25], and cell apoptosis is often accompanied by a decrease in mitochondrial membrane potential (MMP, ΔΨm). Here, we then used the JC-1 fluorescent probe to detect the MMP of ROT-treated SH-SY5Y cells. As shown in Fig. 3A, the ROT-treated cells exhibited more green fluorescence intensity as compared to the untreated cells, indicating a decrease in MMP. However, vidarabine pretreatment remarkably reduced the green fluorescence intensity and increased the red fluorescent intensity in ROT-treated cells (Fig. 3A). Quantitative analysis of the red/green fluorescence ratio of JC-1 indicated that the red/green fluorescence ratio in ROT group was the lowest, while vidarabine pretreatment could significantly increase the red/green fluorescence ratio ($P < 0.05$), suggesting that vidarabine enabled the cells to recover MMP (Fig. 3B).

Mito-Tracker Green is mostly insensitive to MMP and oxidative stress, while Mito-Tracker Red CMXRos can correctly label the active mitochondria. We further performed the mitochondria staining using these two mitochondrial dyes in order to measure the mitochondrial activity and total mitochondrial content of SH-SY5Y cells. Consistent with the previously described partial inhibition of ΔΨm by ROT, the results showed that the total number of mitochondria and the active mitochondria were all reduced in ROT-treated cells, indicating that the mitochondrial activity was affected by ROT (Fig. 3C–E). Vidarabine pretreatment dramatically reduced the ROT-induced loss of total mitochondrial mass and activity, as shown by significant red-green fluorescence intensity (Fig. 3C–E). Moreover, the Mito Red/Mito Green fluorescence intensity ratio, which indicates the number of polarized functional mitochondria, significantly decreased after ROT treatment ($P < 0.01$) (Fig. 3F). However, vidarabine treatment significantly ameliorated the ROT-induced reduction in the ratio of mitotic red/mitotic green fluorescence intensity ($P < 0.05$) (Fig. 3F), suggesting that vidarabine can improve the mitochondrial mass and viability. Taken together, all these results indicated that vidarabine may be able to restore the ROT-induced MMP loss and mitigate the ROT-induced decrease in mitochondrial mass and viability, so as to increase the mitochondrial function in SH-SY5Y cells.

3.4. Vidarabine rescued ROT-induced alterations in mitochondrial morphology rather than the respiratory function defects

Mitochondria often show the abnormal morphological changes in many neurological diseases, including Parkinson's disease [26]. Mito-Tracker RedCMXRos dye was used to specifically label the biologically active mitochondria in cells. Under normal growth conditions, the morphology of mitochondria in neuronal cells is characterized by a well-connected mitochondrial network, as shown in the control group in Fig. 4A. The mitochondrial morphology of ROT-treated SH-SY5Y cells changed from a tubular network to a fractured punctate (circular) structure (Fig. 4A). Notably, the form factor (FF) and aspect ratio (AR) of mitochondria considerably decreased after being treated with ROT in SH-SY5Y cells (Fig. 4B and C). However, after vidarabine treatment (30 μM), the morphological parameters of mitochondria were significantly recovered as compared to the ROT group ($P < 0.01$) (Fig. 4A–C).

The energy necessary to maintain cellular function and survival is often provided by the oxidative phosphorylation (OXPHOS), a major energy conservation process that relates mitochondrial electron transport to ATP production [27]. The evaluation of mitochondrial respiration by detecting the OXPHOS complexes has become an important reference index for drug development strategies for neurodegenerative diseases. Herein, the Seahorse XFp Extracellular Flux Analyzer was used to characterize the mitochondrial function (indicated as oxygen consumption rate; OCR). As shown in Fig. 4D, ROT (0.5 μM) treatment significantly decreased the mitochondrial respiration, consistent with the previous studies the OCR can be almost completely inhibited by ROT over 0.5 μM [28]. However, vidarabine treatment can markedly increase the OCR values at different time points but without significance, suggesting that vidarabine may be not able to directly improve the respiration function of mitochondrial (Fig. 4D and E). Moreover, pre-treatment with vidarabine cannot effectively improve the basal respiration and ATP production (Fig. 4F–I). Thus, vidarabine may be able to rescue the ROT-induced alterations in mitochondrial morphology rather than the respiratory function defects.

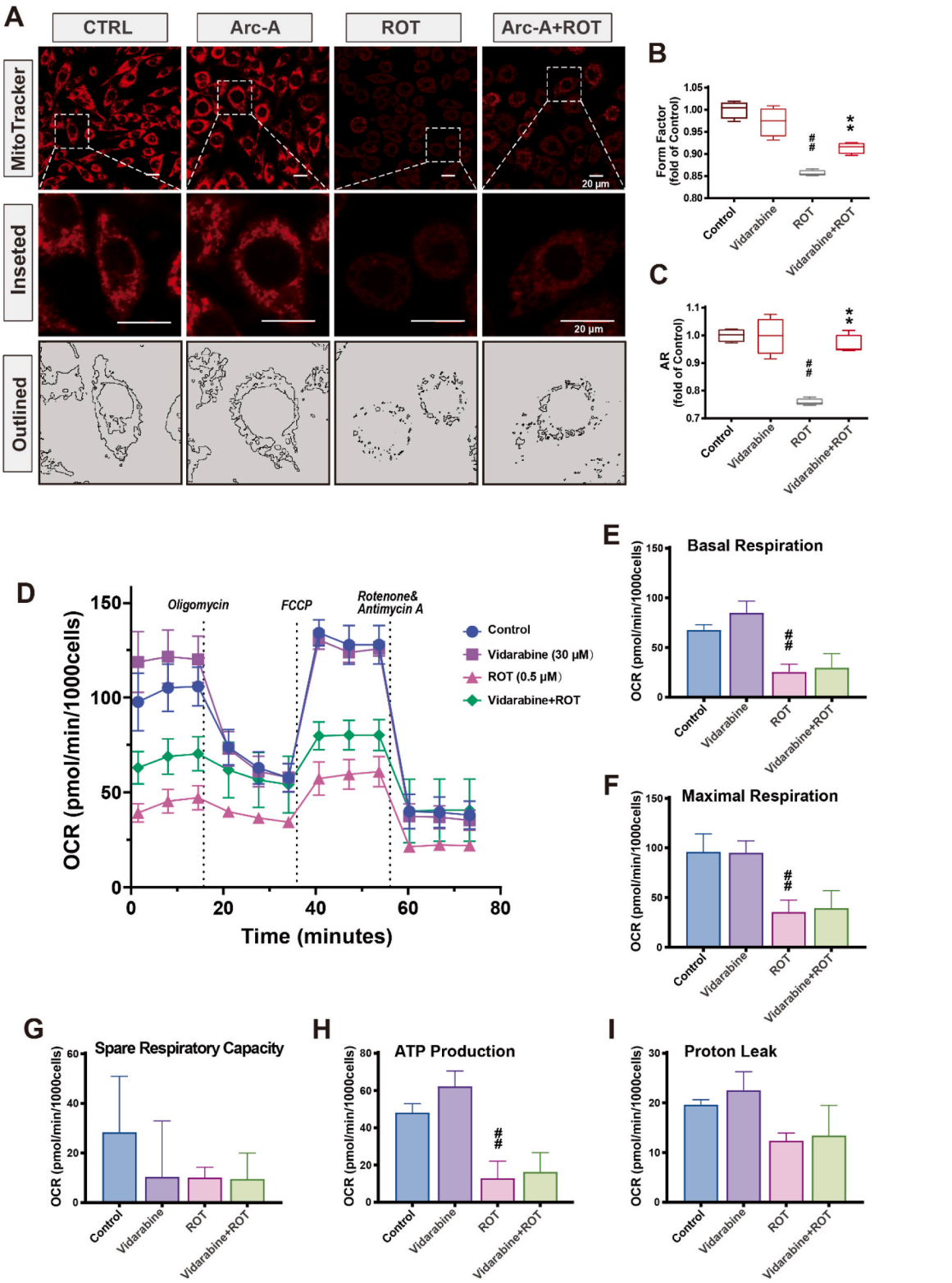

(caption on next page)

Fig. 4. Vidarabine rescued ROT-induced altered mitochondrial morphology rather than the respiratory function. (A) Cells were pretreated with 30 μM vidarabine for 2 h followed by incubation with 20 μM ROT for 24 h. The representative confocal images of mitochondria stained with Mito-Tracker RedCMXRos are shown. Scale bar = 20 μm. (B and C) Quantification of form factor (FF) (B) and aspect ratio (AR) (C) in SH-SY5Y cells. (D) OCR at baseline and after three medications were sequentially injected under various settings. Analysis of basal respiration (E), maximal respiration (F), spare respiratory capacity (G), ATP production (H), and proton leak (I). Data are represented as the mean ± SEM (n = 3), $\#\#P < 0.01$ compared with the control group; $^{**}P < 0.01$ compared with the ROT group.

3.5. Vidarabine promoted the mitochondrial biogenesis in SH-SY5Y cells

The above results indicated that vidarabine possessed a significant mitochondrial protective effect, so we further explored whether it could affect mitochondrial biosynthesis-related signals. We first examined the influence of vidarabine on the protein levels of the PGC-1α/NRF1/TFAM signaling pathway, which plays a critical role in controlling mitochondrial biogenesis [29]. The results showed that ROT treatment significantly reduced the expression levels of PGC-1α, NRF1, and TFAM ($P < 0.01$), as compared to the non-treated control group (Fig. 5A). Vidarabine pretreatment (7.5–30 μM) substantially boosted the expression of PGC-1α, NRF1, and TFAM in a concentration-dependent manner, as compared to the ROT group (Fig. 5A). Thus, vidarabine may increase the process of mitochondrial biogenesis in ROT-induced SH-SY5Y cells via upregulating the levels of PGC-1α, NRF1, and TFAM proteins.

The NAD^+/NADH ratio is currently assumed to be related to the coordination of mitochondrial and nuclear function, as well as the control of energy metabolism. Therefore, we then measured the levels and ratios of NAD^+/NADH to further explore the possible mechanism of vidarabine's neuroprotective effects. As shown in Fig. 5B and C, the NAD^+/NADH level reduced dramatically following ROT treatment, but vidarabine pretreatment (15, 30 μM) significantly increased the NAD^+/NADH ratio ($P < 0.01$), suggesting that vidarabine may be able to restore the ROT-induced decrease.

As a NAD^+-dependent deacetylase, the silent information-regulated transcription factor 1 (SIRT1) can promote mitochondrial biogenesis and function by regulating the transcription of PGC-1α [30]. Since vidarabine increased the NAD^+/NADH ratio, we further examined the effect of vidarabine on the levels of SIRT1 protein. The results indicated that ROT treatment significantly decreased the SIRT1 expression levels ($P < 0.01$), and vidarabine pretreatment (7.5–30 μM) dramatically restored the SIRT1 expression levels in a concentration-dependent manner, consistent with the above results in the evaluation of mitochondrial biogenesis factors. Taken together, all the findings suggested that vidarabine may be able to repair the ROT-induced mitochondrial biogenesis damage and reverse the decrease in the expression levels of the NAD^+-dependent enzyme SIRT1.

3.6. Blocking SIRT1 or mitochondrial biosynthesis attenuates the neuroprotective effects of vidarabine

Since SIRT1 may be involved in the neuroprotective actions of vidarabine, we further explored whether vidarabine might promote mitochondrial biogenesis in a SIRT1-dependent manner to ameliorate ROT-induced mitochondrial damage. So, we examined the effect of vidarabine on mitochondrial biogenesis in ROT-induced SH-SY5Y cells in the presence or absence of EX-527, a selective inhibitor of SIRT1 activity by using Western blot assay and confocal imaging. The cytotoxicity of EX-527 was first evaluated by resazurin assay and the results showed that EX-527 below 20 μM was safe for SH-SY5 cells, and thus 10 μM of EX-527 was used in the subsequent experiments (Fig. 6A). The results of the cell viability assay indicated that addition of EX-527 antagonized the protective effect of vidarabine on ROT-induced cell damage (Fig. 6B). In addition, the results of the YO-PRO-1/PI staining assay indicated that more cell necrosis and apoptosis in both EX-527 and vidarabine-treated SH-SY5 cells as compared to the vidarabine-treated ROT-induced cells (Fig. 6C), further verifying that the SIRT1 activity may be essential for the protective effects of vidarabine.

Moreover, the results of Western blot assay showed that the EX-527 administration inhibited vidarabine-induced activation of SIRT1, accompanied by a decrease in the expression levels of PGC-1α, NRF1, and TFAM proteins (Fig. 6D). Similarly, EX-527 treatment also attenuated the improvement effects of vidarabine on the mitochondrial mass and mitochondrial viability (Fig. 6E), as well as the MMP levels (Fig. 6F). In addition, the shRNA-based knock-down assays were performed to further verify the roles of SIRT1 in the neuroprotective effects of vidarabine. The results showed that the shRNA 2# and 3# can markedly reduce the expression of SIRT1 in SH-SY5Y cells (Fig. S1B), and the SIRT1 knock-down with shRNAs significantly reduced the protective effect of vidarabine on ROT-induced cell damage ($P < 0.01$) (Figs. S1C and S1D). Besides, we also employed a drug affinity responsive target stability (DARTS) assay to detect the potential interaction between vidarabine and SIRT1 protein. The results showed that the SIRT1 protein was obviously protected from thermolysin digestion in the extracts of vidarabine (3 mM) treated cells with or without ROT induction, suggesting that vidarabine may have direct interact with SIRT1 protein in SH-SY5Y cells (Fig. S2). In conclusion, all these results demonstrated that vidarabine may regulate mitochondrial biogenesis through enhancing the SIRT1-dependent PGC-1α/NRF1/TFAM signaling pathway to protect SH-SY5Y cells against ROT-induced mitochondrial dysfunction and neuronal mortality.

3.7. Vidarabine treatment alleviates the motor deficits and neuronal injury in the MPTP-induced PD model mice

To further explore the neuroprotective effects of vidarabine *in vivo*, the MPTP induced nerve injury mouse model was established as described previously (Fig. 7A) [18]. After drug treatment for seven days, a series of behavioral tests were performed to verify the protective role of vidarabine treatment on motor deficits in PD mice. As shown in Fig. 7B, treatment of vidarabine (10 mg/kg/day) significantly attenuated the weight loss in PD model mice as compared to the MPTP control group ($P < 0.05$), but the SIRT1 inhibitor Ex527 treatment (10 mg/kg/day) antagonized the improvement effect of vidarabine on mice weight.

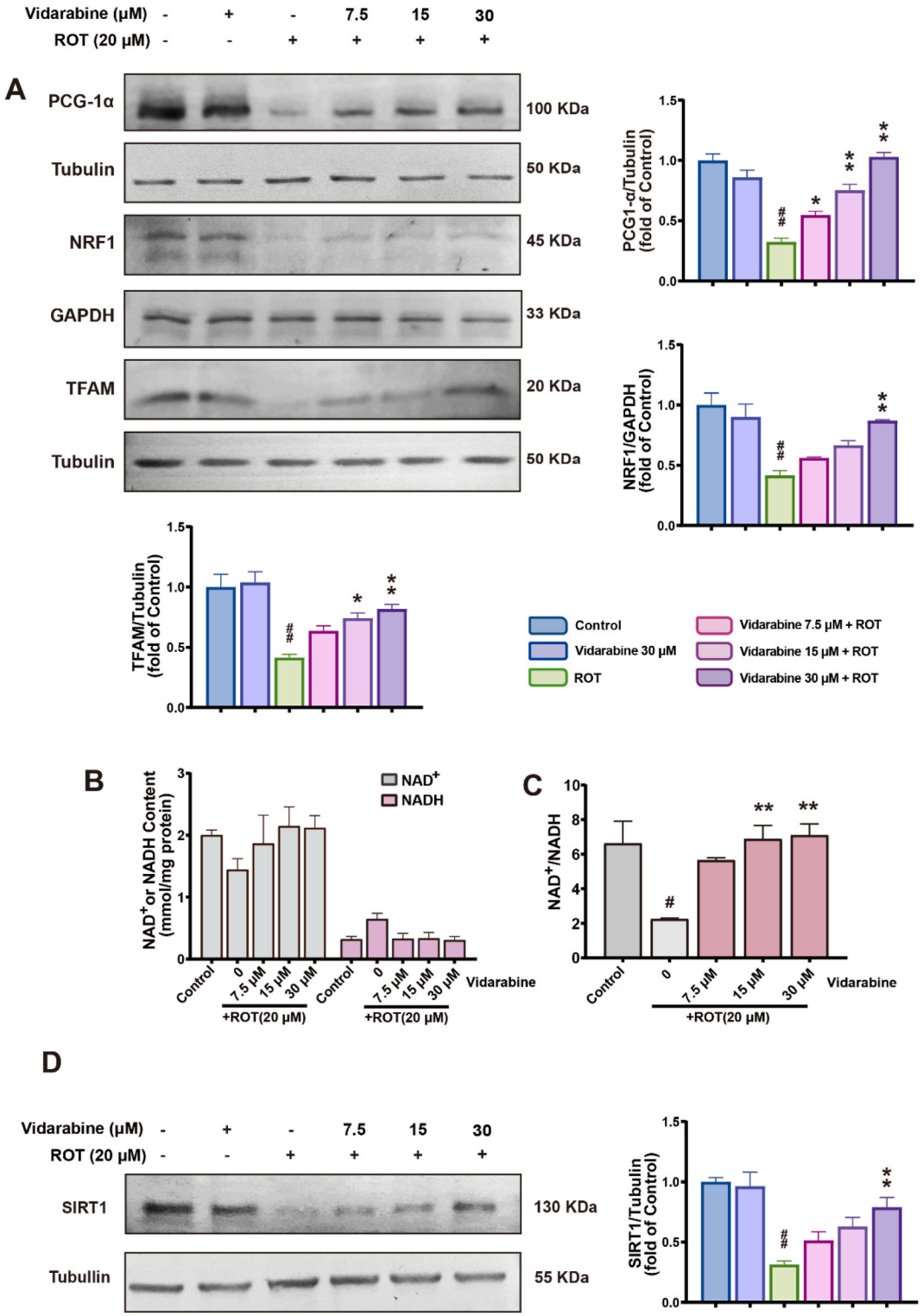

Fig. 5. Vidarabine may promote the mitochondrial biogenesis. (A) Western blot analysis of the expression levels of PGC-1α, NRF1, and TFAM proteins in rotenone (0.5 μM, 24 h) induced SH-SY5Y cells with or without vidarabine pretreatment, and these protein levels were quantified using Image J software. (B and C) The levels of NAD^+ and NADH (B), and the NAD^+/NADH ratio (C) were detected by the NAD^+/NADH assay kit. (D) Western blot analysis was performed to measure the expression levels of SIRT1 protein. Data are represented as the mean ± SEM (n = 3). $\#P < 0.05$, $\#\#P < 0.01$ compared with the control group; $*P < 0.05$, $**P < 0.01$ compared with the ROT group.

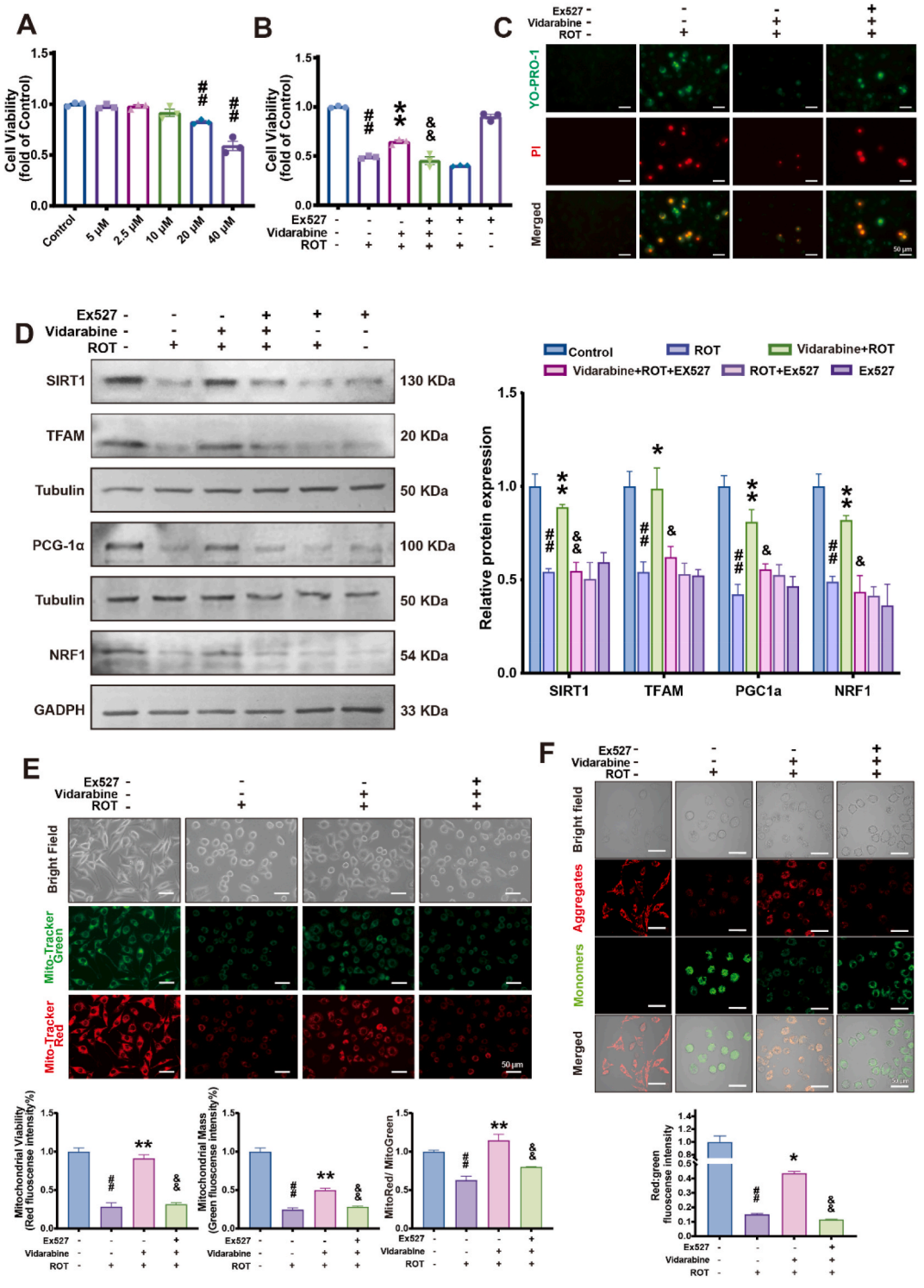

(caption on next page)

Fig. 6. The neuroprotective effect of vidarabine was mediated by SIRT1-dependent PGC-1α/NRF1/TFAM signaling pathway. (A) The cytotoxicity of Ex-527 (Pharmacological inhibitor of SIRT1) in SH-SY5Y cells was measured by the resazurin assay. (B) The influence of Ex-527 on the protective effects of vidarabine on SH-SY5Y cells was determined by the resazurin assay. (C) The effects of Ex-527 and vidarabine on apoptotic and necrotic cells were determined by the YO-PRO-1/PI staining assay under a Fluorescence Microscope. (D) The influence of Ex-527 and vidarabine on the expression levels of SIRT1, PGC-1α, NRF1, and TFAM proteins in ROT-induced SH-SY5Y cells were evaluated by Western blot assay, and these protein levels were quantified using Image J software. (E) The effects of Ex-527 and vidarabine on the mitochondrial mass and mitochondrial viability were determined by using the Mito-Tracker Green and Mito-Tracker Red CMXRos under a Confocal Fluorescence Microscope. Scale bar = 50 μm. (F) The influence of Ex-527 on the changes in the mitochondrial membrane potential (MMP) of SH-SY5Y cells was examined by using the JC-1 staining. Scale bar = 50 μm. Quantification analysis of JC-1 staining was also performed by Image J software. Data are represented as the mean ± SEM (n = 3), ##$P < 0.01$ compared with the control group; *$P < 0.05$, **$P < 0.01$ compared with the ROT group; &$P < 0.05$, &&$P < 0.01$ compared with the Vidarabine + ROT group. (For interpretation of the references to colour in this figure legend, the reader is referred to the Web version of this article.)

Moreover, compared to the non-treated control group, MPTP treatment significantly impaired the motor function, including the reduced mean latency to fall in the traction test, the prolonged time of descend the pole, and the total climbing time in the pole test ($P < 0.05$) (Fig. 7C–E). In contrast, 7-day vidarabine treatment significantly improved the motor deficits in the traction test ($P < 0.05$, Fig. 7C) and reduced the climbing time in the pole test ($P < 0.05$, Fig. 7D and E), suggesting that vidarabine treatment can alleviate the motor deficits in PD mice.

Furthermore, in the open field test, MPTP treatment significantly reduced the travel distance and speed, as compared to the non-treated control group ($P < 0.01$) (Fig. 7F and G). However, treatment of vidarabine significantly increased the travel distance and movement speed ($P < 0.01$), but the SIRT1 inhibitor Ex527 treatment antagonized the improvement effect of vidarabine on motor function (Fig. 7F and G). Besides, vidarabine treatment can also significantly increase the number of crossing lines and movement time in the open field test (Fig. 7H and I). In addition, MPTP treatment also induced the neuronal cell injury, including the disordered neuronal arrangement and the neuron relaxation and edema (Fig. 7J). In contrast, vidarabine treatment markedly attenuated the neuropathic symptoms while the SIRT1 inhibitor Ex527 antagonized the improvement effect of vidarabine on neuronal injury (Fig. 7J). Taken together, vidarabine also possesses significant neuroprotective effect in PD mice, which may largely depend on the roles of SIRT1.

4. Discussion

Until now, there is still a lack of therapeutic measures to block or postpone PD neurodegeneration, thus it is necessary to develop novel therapeutic drugs for the prevention and therapy of PD. In this study, we found that the marine derived compound vidarabine possessed significant neuroprotective effects against rotenone (ROT) induced SH-SY5Y cell injury. Vidarabine was first licensed by the FDA as an anti-herpes virus agent for widespread clinical use, now been integrated into a broader variety of research during the last decade. Herein, we found that vidarabine may be able to notably increase the mitochondrial biogenesis and improve subsequent mitochondrial function by activating t the SIRT1-dependent PGC-1α/NRF1/TFAM signaling pathway to prevent ROT-induced neurotoxicity (Fig. 8).

The precise mechanisms by which neurodegeneration leads to PD progression, although still elusive, are known to involve the overproduction of ROS, mitochondrial and lysosomal dysfunction, neuroinflammation, and environmental toxins [31]. Oxidative stress and mitochondrial dysfunction are reported to be predominantly involved in the pathophysiology of PD [32]. Among them, Mitochondrial dysfunction and oxidative stress are interdependent because excess ROS produced by oxidative stress causes the accumulation of mutant and damaged mtDNA, while the mutations in mtDNA in turn can result in mitochondrial malfunction, which intensifies oxidative damage [2,33]. In this study, vidarabine pretreatment can attenuate ROT-induced oxidative stress damage by increasing the antioxidant capacity and enzyme activity such as SOD and GSH, suggesting that vidarabine may be able to prevent neuronal cell damage via inhibiting ROS-mediated oxidative stress.

In PD patients, abnormal alpha-syn and toxins accumulate at the mitochondrial electron transport chain complex I, causing it to malfunction [34]. Besides, because the majority of hereditary PD loci are directly linked to mitochondria [35], mitochondrial dysfunction is regarded as a holistic disease component in PD and an activator of dopaminergic neuronal degeneration. Our findings showed that vidarabine significantly reduced the ROT-induced decrease in mitochondrial mass and viability, prevented the decrease in MMP, and restored the mitochondrial morphology and function, implying that vidarabine's neuroprotection is closely related to the inhibition of mitochondrial damage, protection of mitochondrial function, and improvement of energy metabolism. In addition, NAD^+ is a coenzyme that is essential for energy balance and cellular redox processes, which plays a role in neurodegenerative diseases [35]. In this study, ROT reduced NAD^+ levels in SH-SY5Y cells, leading to a reduction in NAD^+/NADH. vidarabine reversed this transition by balancing the NAD^+/NADH ratio, which is directly connected to the improved activity of mitochondrial complex I. Thus, vidarabine might also exert mitochondria-protective effects by maintaining the mitochondrial NAD^+ pool and restoring the NAD^+/NADH equilibrium.

There is growing evidence that neurodegenerative diseases may be caused by impaired mitochondrial biogenesis, particularly at the level of PGC-1α. PGC-1α overexpression can protect the DA neurons and mitochondrial homeostasis while also increasing the antioxidant expression [36,37]. PGC-1α and its target genes such as NRF-1 and TFAM are all downregulated in PD patients. PGC-1α expression, on the other hand, has been found to inhibit -Syn oligomerization and preserve DA neurons [38]. PGC-1α increases the expression levels and activity of NRF1 and NRF2, which activate TFAM to bind to the promoter regions of nuclear genes which can

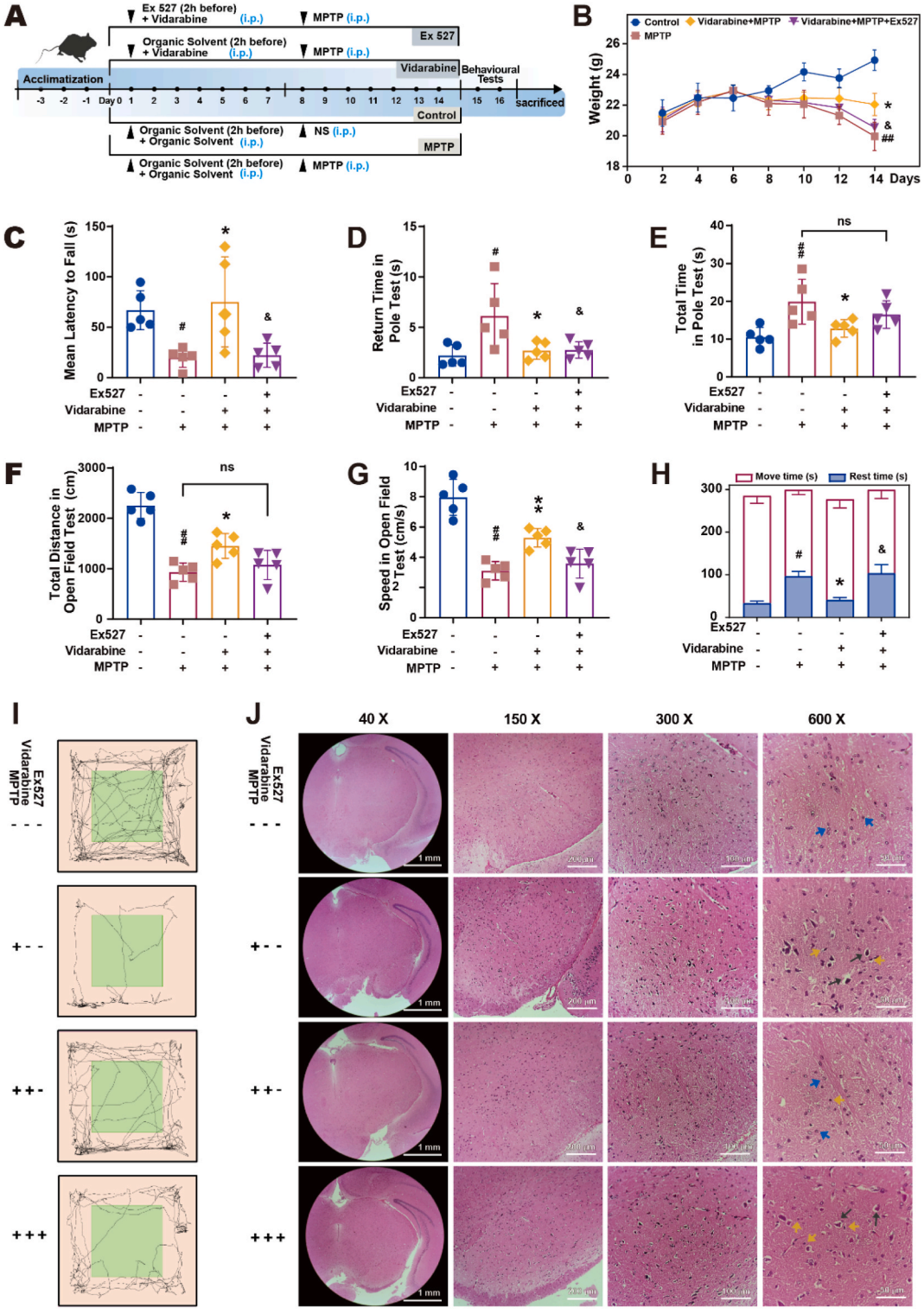

(caption on next page)

Fig. 7. Vidarabine treatment alleviated the motor deficits and neuronal injury in the MPTP-induced PD mouse model. (A) Schematic representation for the experimental procedure. (B) The change of average body weight in MPTP-induced PD mice. (C) The mean latency to fall in the traction test. (D and E) The return time (D) and total time (E) of descend the pole in the pole test. (F and G) The total travel distance (F) and movement speed (G) in the open field test. (H and I) The movement time (H) and number of crossing lines (I) in the open field test. (J) Histopathology analyses of brain tissues by HE staining (× 40, × 150, × 300, and × 600). The representative micrographs from each group were shown. The blue and yellow arrows indicate the neuropathic symptoms. Data are represented as the mean ± SEM (n = 5). $\#P < 0.05$, $\#\#P < 0.01$ compared with the control group; $*P < 0.005$, $**P < 0.01$ compared with the ROT group; $\&P < 0.05$ compared with the Vidarabine + ROT group. (For interpretation of the references to colour in this figure legend, the reader is referred to the Web version of this article.)

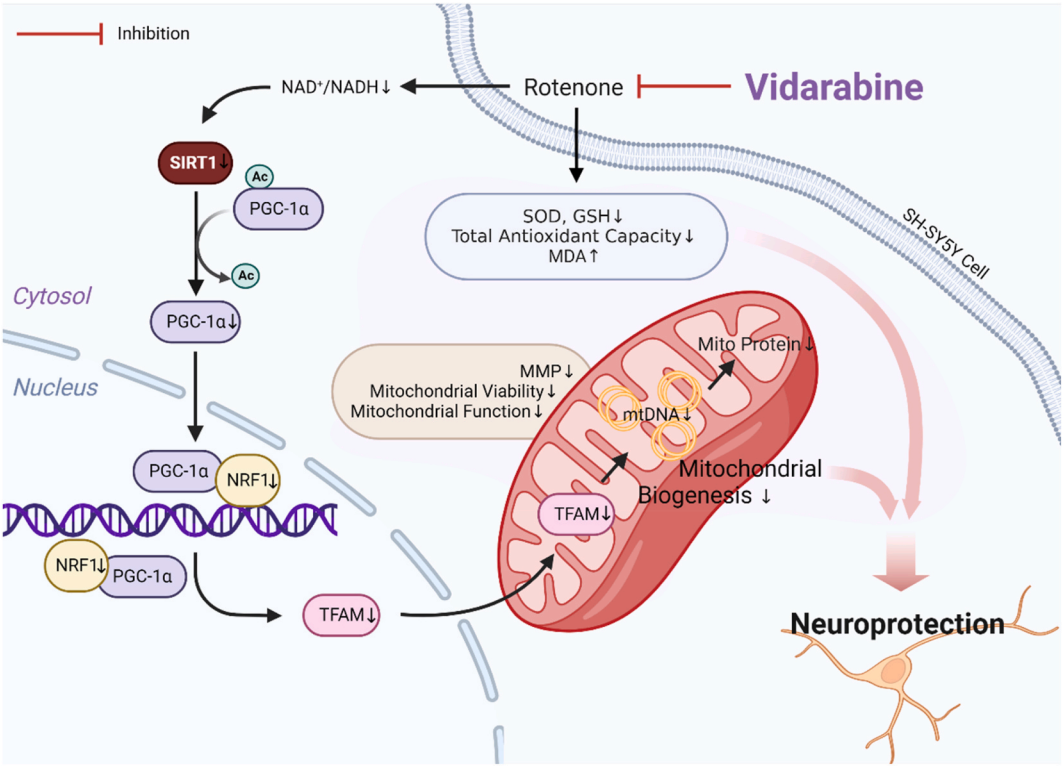

Fig. 8. A proposed model underlying the protective mechanisms of vidarabine against ROT induced neuronal damage. Vidarabine plays an important role in avoiding ROT-induced neurotoxicity via its abilities to lower the oxidative stress and rescue the mitochondrial dysfunction. Vidarabine may also enhance the SIRT1-dependent PGC-1α/NRF1/TFAM signaling pathway to improve mitochondrial biogenesis so as to further minimize neuronal apoptosis. Created with BioRender.com.

increase the assembly of the respiratory apparatus and ultimately generating new mitochondria [6]. In the present study, we found a significant attenuation effect of vidarabine on the reduction of PGC-1α and TFAM induced by ROT injury, suggesting that vidarabine may be able to promote mitochondrial biogenesis through upregulation of PGC-1α and TFAM.

Two important signaling pathways that govern mitochondrial biogenesis are the AMP-activated kinase (AMPK)-PGC1α axis and the sirtuin 1 (SIRT1)-PGC1α axis [27,39]. Considering that vidarabine increased the levels of NAD^+ and NAD^+/NADH, and the sirtuins are NAD^+-dependent deacetylase, as well as SIRT1 is a critical regulator of mitochondrial biogenesis [40], we hypothesized that SIRT1 may be the upstream signaling molecule of vidarabine-mediated mitochondrial biogenesis in neurons. In this study, we used the SIRT1 inhibitor EX-527 to block the expression of SIRT1 in order to verify the key roles of SIRT1. Interestingly, EX-527 can truly inhibit the PGC-1α/NRF1/TFAM signaling pathway and impair the mitochondrial biogenesis, thereby reversing the protective effects of vidarabine against ROT-induced mitochondrial dysfunction and cell death. Besides, the SIRT1 knock-down with shRNAs significantly reduced the protective effect of vidarabine on ROT-induced cell damage, verifying the key roles of SIRT1 in the neuroprotective effects of vidarabine. The DARTS assay indicated that vidarabine treatment can protect the SIRT1 protein from protease digestion in the presence or absence of ROT induction, suggesting that vidarabine may have direct interact with SIRT1 in SH-SY5Y cells. Taken together, these results suggested that vidarabine may prevent ROT-induced neurotoxicity through the activation of mitochondrial biogenesis regulated by the SIRT1-dependent PGC-1α/NRF1/TFAM signaling pathway.

The *in vitro* neuroprotective effects of vidarabine were mirrored in the MPTP induced PD mice model. Herein, we found that intraperitoneal injection of vidarabine (10 mg/kg/day) significantly attenuated the weight loss and alleviated the motor deficits in the pole test, traction test and the open field test. Vidarabine treatment also significantly attenuated the neuronal injury symptoms such as

the neuron depression and edema in brain, suggesting that vidarabine also possesses marked neuroprotective effects in PD mice (Fig. 7). Besides, the SIRT1 inhibitor Ex527 can antagonize the improvement effects of vidarabine on neuronal injury, suggesting that the neuroprotective effect of vidarabine *in vivo* may also depend on the roles of SIRT1. Thus, vidarabine may be used for prevention and therapy of neuronal disorders targeting SIRT1 in the future.

5. Conclusion

In conclusion, our findings revealed that the marine-derived medicine vidarabine can dramatically improve the mitochondrial dysfunction in PD models *in vitro* and *in vivo*. We discovered for the first time that this favorable effect may be mediated by mitochondrial biogenesis via the PGC-1α/NRF1/TFAM signaling pathway. The neuroprotective characteristics of this molecule revealed in this work, together with the acceptable safety and pharmacokinetic profiles reported in clinical trials, imply that vidarabine might serve as a valuable alternative treatment candidate for PD shortly. Thus, vidarabine merits further investigation to be developed into a novel prophylactic or therapeutic agent against PD and other neuronal disorders targeting SIRT1-dependent mitochondrial biogenesis.

Funding

This work was supported by National Natural Science Foundation of China (31500646), Shandong Provincial Natural Science Foundation (ZR2023MH185), Qingdao Natural Science Foundation (23-2-1-168-zyyd-jch), and Youth Research Fund of the Affiliated Hospital of Qingdao University (QDFYQN202101003).

Institutional review board statement

Not applicable.

Informed consent statement

Not applicable.

Data availability statement

The data that support the findings of this study are available from the corresponding author upon reasonable request.

Declaration of competing interest

The authors declare that they have no known competing financial interests or personal relationships that could have appeared to influence the work reported in this paper.

Appendix A. Supplementary data

Supplementary data to this article can be found online at https://doi.org/10.1016/j.heliyon.2023.e21695.

References

[1] B.R. Bloem, et al., Parkinson's disease, Lancet 397 (10291) (2021) 2284–2303, https://doi.org/10.1016/s0140-6736(21)00218-x.
[2] P.A. Dionísio, et al., Oxidative stress and regulated cell death in Parkinson's disease, Ageing Res. Rev. 67 (2021), 101263, https://doi.org/10.1016/j.arr.2021.101263.
[3] M.A. Eldeeb, et al., Mitochondrial quality control in health and in Parkinson's disease, Physiol. Rev. 102 (4) (2022) 1721–1755, https://doi.org/10.1152/physrev.00041.2021.
[4] J.J. Collier, et al., Mitochondrial signalling and homeostasis: from cell biology to neurological disease, Trends Neurosci. 46 (2) (2023) 137–152, https://doi.org/10.1016/j.tins.2022.12.001.
[5] A.P. Gureev, et al., Regulation of mitochondrial biogenesis as a way for active longevity: interaction between the Nrf2 and PGC-1α signaling pathways, Front. Genet. 10 (2019), https://doi.org/10.3389/fgene.2019.00435.
[6] F.R. Jornayvaz, G.I. Shulman, Regulation of mitochondrial biogenesis, Essays Biochem. 47 (2010) 69–84, https://doi.org/10.1042/bse0470069.
[7] R.C. Scarpulla, Transcriptional paradigms in mammalian mitochondrial biogenesis and function, Physiol. Rev. 88 (2) (2008) 611–638, https://doi.org/10.1152/physrev.00025.2007.
[8] S. Sagar, et al., Antiviral lead compounds from marine sponges, Mar. Drugs 8 (10) (2010) 2619–2638, https://doi.org/10.3390/md8102619.
[9] E. Cappello, P. Nieri, From life in the sea to the clinic: the marine drugs approved and under clinical trial, Life-Basel 11 (12) (2021) 1390, https://doi.org/10.3390/life11121390.
[10] K. Iwatsubo, et al., Prevention of heart failure in mice by an antiviral agent that inhibits type 5 cardiac adenylyl cyclase, Am J Physiol-Heart C 302 (12) (2012) H2622–H2628, https://doi.org/10.1152/ajpheart.00190.2012.
[11] M.S. De Lorenzo, et al., Reduced malignancy as a mechanism for longevity in mice with adenylyl cyclase type 5 disruption, Aging Cell 13 (1) (2013) 102–110, https://doi.org/10.1111/acel.12152.

[12] K. Suita, et al., Vidarabine, an anti-herpesvirus agent, prevents catecholamine-induced arrhythmias without adverse effect on heart function in mice, Pflug Arch Eur J Phy 470 (6) (2018) 923–935, https://doi.org/10.1007/s00424-018-2121-4.
[13] K. Präbst, et al., Basic colorimetric proliferation assays: mtt, wst, and resazurin, in: Methods in Molecular Biology, Springer, New York, 2017, pp. 1–17.
[14] T. Idziorek, et al., Yopro-1 permits cytofluorometric analysis of programmed cell death (apoptosis) without interfering with cell viability, J. Immunol. Methods 185 (2) (1995) 249–258, https://doi.org/10.1016/0022-1759(95)00172-7.
[15] W. Pendergrass, et al., Efficacy of mitotracker green? And cmxrosamine to measure changes in mitochondrial membrane potentials in living cells and tissues, Cytometry 61A (2) (2004) 162–169, https://doi.org/10.1002/cyto.a.20033.
[16] M. Poot, et al., Analysis of mitochondrial morphology and function with novel fixable fluorescent stains, J. Histochem. Cytochem. 44 (12) (1996) 1363–1372, https://doi.org/10.1177/44.12.8985128.
[17] W.J.H. Koopman, et al., Inhibition of complex I of the electron transport chain causes O2-. -mediated mitochondrial outgrowth, Am J Physiol-Cell Ph 288 (6) (2005) C1440–C1450, https://doi.org/10.1152/ajpcell.00607.2004.
[18] Z. Jiang, et al., β-Hydroxybutyrate alleviates pyroptosis in MPP+/MPTP-induced Parkinson's disease models via inhibiting STAT3/NLRP3/GSDMD pathway, Int. Immunopharm. 113 (Pt B) (2022), 109451, https://doi.org/10.1016/j.intimp.2022.109451.
[19] Z.L. Zhou, et al., Neuroprotection of fasting mimicking diet on MPTP-induced Parkinson's disease mice via gut microbiota and metabolites, Neurotherapeutics 16 (3) (2019) 741–760, https://doi.org/10.1007/s13311-019-00719-2.
[20] J. Sun, et al., Probiotic Clostridium butyricum ameliorated motor deficits in a mouse model of Parkinson's disease via gut microbiota-GLP-1 pathway, Brain Behav. Immun. 91 (2021) 703–715, https://doi.org/10.1016/j.bbi.2020.
[21] C. Hao, et al., The neuroprotective effects of peracetylated chitosan oligosaccharides against beta-amyloid-induced cognitive deficits in rats, Mar Life Sci Technol 5 (2) (2023) 211–222, https://doi.org/10.1007/s42995-023-00172-3.
[22] J.W. Gnann, M.R. Salvaggio, Drugs for herpesvirus infections, in: Infectious Diseases, Elsevier, 2010, pp. 1454–1463.
[23] T.B. Sherer, et al., An in vitro model of Parkinson's disease: linking mitochondrial impairment to altered α-synuclein metabolism and oxidative damage, J. Neurosci. 22 (16) (2002) 7006–7015, https://doi.org/10.1523/jneurosci.22-16-07006.2002.
[24] O. Hwang, Role of oxidative stress in Parkinson's disease, Exp Neurobiol 22 (1) (2013) 11–17, https://doi.org/10.5607/en.2013.22.1.11.
[25] N.N. Danial, S.J. Korsmeyer, Cell death, Cell 116 (2) (2004) 205–219, https://doi.org/10.1016/s0092-8674(04)00046-7.
[26] G. Cenini, et al., Oxidative stress in neurodegenerative diseases: from a mitochondrial point of view, Oxid. Med. Cell. Longev. 2019 (2019) 1–18, https://doi.org/10.1155/2019/2105607.
[27] C. Huang, et al., Mitochondrial cristae in health and disease, Int. J. Biol. Macromol. 235 (2023), 123755, https://doi.org/10.1016/j.ijbiomac.2023.123755.
[28] H. Bai, et al., Polydatin protects SH-SY5Y in models of Parkinson's disease by promoting Atg5-mediated but parkin-independent autophagy, Neurochem. Int. 134 (2020), 104671, https://doi.org/10.1016/j.neuint.2020.104671.
[29] L.D. Popov, Mitochondrial biogenesis: an update, J. Cell Mol. Med. 24 (9) (2020) 4892–4899, https://doi.org/10.1111/jcmm.15194.
[30] G.E.-S. Batiha, et al., Sirt1 pathway in Parkinson's disease: a faraway snapshot but so close, Inflammopharmacology 31 (1) (2022) 37–56, https://doi.org/10.1007/s10787-022-01125-5.
[31] D.C. Xu, et al., Signaling pathways in Parkinson's disease: molecular mechanisms and therapeutic interventions, Signal Transduct Tar 8 (1) (2023) 73, https://doi.org/10.1038/s41392-023-01353-3.
[32] E.O. Olufunmilayo, et al., Oxidative stress and antioxidants in neurodegenerative disorders, Antioxidants-Basel 12 (2) (2023) 517, https://doi.org/10.3390/antiox12020517.
[33] L. Devi, et al., Mitochondrial import and accumulation of α-synuclein impair complex i in human dopaminergic neuronal cultures and Parkinson disease brain, J. Biol. Chem. 283 (14) (2008) 9089–9100, https://doi.org/10.1074/jbc.m710012200.
[34] F. Jia, et al., Monogenic Parkinson's disease: genotype, phenotype, pathophysiology, and genetic testing, Genes-Basel 13 (3) (2022) 471, https://doi.org/10.3390/genes13030471.
[35] N. Koju, et al., Reduced nicotinamide adenine dinucleotide phosphate in redox balance and diseases: a friend or foe? Acta Pharmacol. Sin. 43 (8) (2022) 1889–1904, https://doi.org/10.1038/s41401-021-00838-7.
[36] E. Di Giacomo, et al., Roles of ppar transcription factors in the energetic metabolic switch occurring during adult neurogenesis, Cell Cycle 16 (1) (2017) 59–72, https://doi.org/10.1080/15384101.2016.1252881.
[37] E. Piccinin, et al., Pgc-1s in the spotlight with Parkinson's disease, Int. J. Mol. Sci. 22 (7) (2021) 3487, https://doi.org/10.3390/ijms22073487.
[38] C. Ciron, et al., PGC-1α activity in nigral dopamine neurons determines vulnerability to α-synuclein, Acta Neuropathol Com 3 (1) (2015), https://doi.org/10.1186/s40478-015-0200-8.
[39] C. Cardanho-Ramos, V.A. Morais, Mitochondrial biogenesis in neurons: how and where, Int. J. Mol. Sci. 22 (23) (2021), 13059, https://doi.org/10.3390/ijms222313059.
[40] F.A. Lagunas-Rangel, Sirt7 in the aging process, Cell. Mol. Life Sci. 79 (6) (2022) 297, https://doi.org/10.1007/s00018-022-04342-x.